CrossMark

JM PAPERS

Scaling the self-propulsive performance of pitching and heaving flexible plates

Kui Liu[1], **Xuechao Liu**[1] **and Haibo Huang**[1],†

[1]Department of Modern Mechanics, University of Science and Technology of China, Hefei, Anhui 230026, PR China

Self-propulsive performances of the flexible plates undergoing pitching and heaving motions are investigated numerically. The effects of multiple key dimensionless parameters are considered, such as bending stiffness, heaving amplitude, pitching amplitude and flapping frequency. Despite so many influence factors, results indicate that the cruising speed U (or the cruising Reynolds number Re_c), the thrust T and the input power P can be summarized as some simple scaling laws vs the flapping Reynolds number Re_f. In the heaving motion, the scaling laws may be not fully independent of bending stiffness because in the motion the role of bending stiffness is more complicated for the thrust generation. Our scaling laws are well supported by biological data on swimming aquatic animals.

Key words: flow-structure interactions, swimming/flying, propulsion

1. Introduction

In nature, birds, insects and fish utilize flapping wings or fins to generate thrust for locomotion. Related issues intrigue lots of researchers and considerable breakthroughs and advances have been achieved over the past few decades through experimental measurements, theoretical analysis and numerical modelling (Triantafyllou, Triantafyllou & Yue 2000; Lauder 2015; Smits 2019). These advances are useful not only to biologists for better understanding of the underlying biology of fish and aquatic mammals, but also to engineers for the design of efficient biomimetic underwater vehicles (Dai *et al.* 2018; Smits 2019; Lin, Wu & Zhang 2021).

Previous studies have focused on the scaling laws of swimming performances (e.g. thrust and power expenditure). Quinn *et al.* (2014) investigated a rigid tethered pitching foil near a solid boundary through experiments and numerical simulations at a chord-based Reynolds number (*Re*) of approximately 4700. They have shown that the thrust *T* can be

† Email address for correspondence: huanghb@ustc.edu.cn

scaled as $(fA_t)^2$ and the power input P can be scaled as $(fA_t)^{2.7}$ if the foil is far from the ground, where f and A_t are the flapping frequency and the amplitude of the trailing edge, respectively. Floryan *et al.* (2017) studied rigid tethered pitching and heaving foils by experiments on a nominally two-dimensional flow with $Re = 4780$. They found that the foil performances depend on the Strouhal number and reduced frequency. Further, they proposed that the thrust scaling is $T \sim (fA_t)^2$ if the offset drag is negligible (Floryan, Van Buren & Smits 2018), which is consistent with Quinn *et al.* (2014). They also suggested that the power scaling is $P \sim fL(V^2 - V_h V_\theta)$ (Floryan *et al.* 2018), where L is the length of the propulsor, $V = fA_t$ is the characteristic speed of the transverse motion, and $V_h = fh_0$ and $V_\theta = fL\theta_0$ are the transverse velocity scales characteristic of the heaving and pitching motions, respectively. The thrust scaling $T \sim (fA_t)^2$ is also derived by Gazzola, Argentina & Mahadevan (2014) through theoretical analysis and they also found that the cruising Reynolds number Re_c can be scaled as $Re_f^{4/3}$, where $Re_c = UL/\nu$ based on the cruising speed U, and $Re_f = 2\pi fA_t L/\nu$ is the flapping Reynolds number (also termed as the swimming number) (Vandenberghe, Zhang & Childress 2004; Gazzola *et al.* 2014). Here ν is the kinematic viscosity of the fluid. By numerical simulations of rigid unconstrained pitching foils, Lin *et al.* (2021) indicated that $Re_c \sim Re_f^{5/3}$ based on a new thrust scaling $T \sim (fA_t)^{5/2}$. Nevertheless, this new thrust scaling has never been confirmed or validated yet.

However, the rigid foils are quite different from the real wings/fins of birds/fish. These flapping wings/fins undergo large active or passive deformation in nature (Wootton 1992; Lauder 2015). Evidence has shown that flexibility has significant effect on the performance of the propeller (Thiria & Godoy-Diana 2010; Kang *et al.* 2011; Marais *et al.* 2012; Shoele & Zhu 2012; Zhu, He & Zhang 2014b; Floryan & Rowley 2018; Peng, Huang & Lu 2018a). For instance, the thrust for the tethered pitching flexible foil is found to be up to three times larger than that of the rigid foil (Marais *et al.* 2012) and for the self-propulsive heaving flexible plate, the propulsive efficiency is much higher under certain conditions compared with the rigid plate (Zhu *et al.* 2014b). In addition, the self-propelled flexible flapping wing may take on a more aerodynamic shape to achieve high efficiency (Ramananarivo, Godoy-Diana & Thiria 2011). Dewey *et al.* (2013) experimentally studied the performances of pitching flexible panels at $Re \approx 7200$ and found that the global maximum efficiency for the flexible panels is twice as much as that of the rigid panels.

Besides, the drag experienced by a flexible body is quite different from that of a rigid body. Alben, Shelley & Zhang (2002, 2004) showed that a flexible body experiences a drag proportional to $U^{4/3}$ by experiments and theoretical analysis with Re in the range 2000–40 000. Neither $U^{3/2}$ scaling of a flat plate aligned with the flow (Gazzola *et al.* 2014), nor classical U^2 drag scaling of rigid bodies (Batchelor 1967) is applicable to the flexible body. This means that a flexible body can achieve drag reduction through self-similar bending or shape deformations due to flexibility (Alben *et al.* 2002). Later, Zhu (2008) numerically studied the same problem as Alben *et al.* (2002) and found that the 4/3 power law of drag also occurs at lower Re (≈ 800). The $U^{4/3}$ drag scaling of a flexible body has also been confirmed by other studies further (Gosselin, de Langre & Machado-Almeida 2010; Luhar & Nepf 2011).

It is noteworthy that, in the experimental studies mentioned above, the object is fixed in an oncoming flow and cannot propel themselves freely. Although Van Buren *et al.* (2018) suggested that tethered studies can be used to make robust conclusions about swimming performance, the self-propelled study may be better since the dynamic response of the swimmer to the surrounding flow is considered. In the present study, the performances of self-propelled flexible plates are investigated numerically. The plate can move freely in
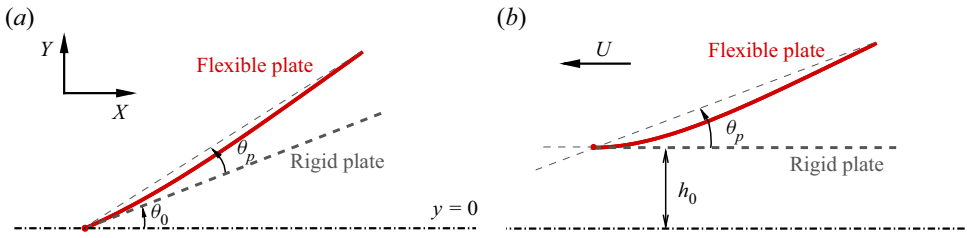
Figure 1. Schematic diagram of the (*a*) pitching and (*b*) heaving flexible plates. The red curved lines represent the flexible plates and the thick dashed lines represent the rigid plates. Here θ_0 and h_0 are the active pitching and heaving amplitudes, respectively, and θ_p is the passive pitching angle associated with the deformation of the flexible plate.

the propulsion direction. Two locomotion styles are considered, namely, the pitching and heaving motions. Meanwhile, the bending stiffness, the flapping amplitude and frequency are variable and their corresponding effects are investigated. We mainly focus on the scaling laws for propulsive speed, thrust and input power of the plates.

The remainder of this paper is organized as follows. The physical problem and mathematical formulation are presented in § 2. The numerical method and validation are described in § 3. Detailed results are discussed in § 4 and concluding remarks are addressed in § 5.

2. Physical problem and mathematical formulation

The schematic diagram of pitching and heaving flexible plates that we considered are shown in figure 1. The leading edge of the plate is forced to pitch (figure 1*a*) and heave (figure 1*b*) in the lateral direction, respectively. The motions are described as

$$\theta(t) = \theta_0 \sin(2\pi f t), \tag{2.1}$$

$$h(t) = h_0 \sin(2\pi f t), \tag{2.2}$$

where $\theta(t)$ and $h(t)$ are the instantaneous pitching and heaving motions, respectively, θ_0 and h_0 are the pitching and heaving amplitudes, respectively, and f is the flapping frequency.

Note that only the leading edge of the plate is restricted with the prescribed lateral motion while other parts of the plate can move freely due to fluid–structure interaction. It is noticed that for the heaving motion, there is no active pitching but the plate may pitch passively.

The incompressible Navier–Stokes equations are adopted to solve the fluid flow:

$$\frac{\partial \boldsymbol{v}}{\partial t} + \boldsymbol{v} \cdot \nabla \boldsymbol{v} = -\frac{1}{\rho} \nabla p + \frac{\mu}{\rho} \nabla^2 \boldsymbol{v} + \boldsymbol{f}_b, \tag{2.3}$$

$$\nabla \cdot \boldsymbol{v} = 0, \tag{2.4}$$

where $\boldsymbol{v}$ is the velocity, p is the pressure, ρ is the density of the fluid, μ is the dynamic viscosity and $\boldsymbol{f}_b$ is the Eulerian momentum force acting on the surrounding fluid due to the immersed boundary. To enforce the no-slip boundary condition, a virtual force is applied to each Lagrange point of the immersed boundary (Peskin 2002; Mittal & Iaccarino 2005). The virtual force is distributed to the surrounding neighbouring fluid nodes through a delta function, i.e. at a relevant fluid node, there is a non-zero $\boldsymbol{f}_b$. It is noticed that at most fluid nodes far away from the Lagrange points, $\boldsymbol{f}_b = 0$.

936 A9-3

The structural equation is employed to describe the deformation and motion of the plate (Zhu & Peskin 2002; Connell & Yue 2007; Hua, Zhu & Lu 2013):

$$\rho_l \frac{\partial^2 X}{\partial t^2} - \frac{\partial}{\partial s}\left[Eh\left(1 - \left|\frac{\partial X}{\partial s}\right|^{-1}\right)\frac{\partial X}{\partial s}\right] + EI\frac{\partial^4 X}{\partial^4 s} = F_s, \tag{2.5}$$

where s is the Lagrangian coordinate along the plate, ρ_l is the structural linear mass density, $X(s, t) = (X(s, t), Y(s, t))$ is the position vector of the plate, F_s is the Lagrangian force exerted on the plate by the surrounding fluid. Here Eh and EI denote the structural stretching rigidity and bending rigidity, respectively. At the leading edge of the plate, for the heaving motion, the clamped boundary condition is adopted, i.e.

$$-Eh\left(1 - \left|\frac{\partial X}{\partial s}\right|^{-1}\right)\frac{\partial X}{\partial s} + EI\frac{\partial^3 X}{\partial^3 s} = 0, \quad Y(t) = h(t), \quad \frac{\partial X}{\partial s} = (1, 0), \tag{2.6a–c}$$

while for the pitching motion, the boundary condition is expressed as

$$-Eh\left(1 - \left|\frac{\partial X}{\partial s}\right|^{-1}\right)\frac{\partial X}{\partial s} + EI\frac{\partial^3 X}{\partial^3 s} = 0, \quad Y(t) = 0, \quad \frac{\partial X}{\partial s} = (\cos\theta, \sin\theta). \tag{2.7a–c}$$

Note that the first boundary condition in (2.6a–c) and (2.7a–c) represents the horizontally unconstrained condition. At the free end, the boundary condition is expressed as

$$-Eh\left(1 - \left|\frac{\partial X}{\partial s}\right|^{-1}\right)\frac{\partial X}{\partial s} + EI\frac{\partial^3 X}{\partial^3 s} = 0, \quad \frac{\partial^2 X}{\partial s^2} = 0. \tag{2.8a,b}$$

In addition, $X(s, 0) = (s, y(0))$, $\partial X/\partial t(s, 0) = (0, 0)$ are the initial conditions for the plate.

In our study, the fluid density ρ, the dynamic viscosity μ, the dimensional length of the plate L and the Reynolds number ($Re = 200$) are fixed. To normalize the above equations, the characteristic quantities ρ, L and U_{ref} are chosen where $U_{ref} = \mu Re/(\rho L)$. Therefore, the characteristic time is $T_{ref} = L/U_{ref}$. Based on dimensional analysis, the following dimensionless governing parameters are introduced: the heaving amplitude h_0^*, the pitching amplitude θ_0, the flapping frequency f^*, the Reynolds number $Re = \rho U_{ref}L/\mu$, the mass ratio of the plate to the fluid $M^* = \rho_l/(\rho L)$, the stretching stiffness $S^* = Eh/(\rho U_{ref}^2 L)$ and the bending stiffness $K^* = EI/(\rho U_{ref}^2 L^3)$.

3. Numerical method and validation

The governing equations of the fluid–plate problem are solved numerically by an immersed boundary-lattice Boltzmann method for the fluid flow and a finite element method for the motion of the flexible plate. The body force term f_b in (2.3) represents an interaction force between the fluid and the immersed boundary to enforce the no-slip velocity boundary condition. Equation (2.5) for the plate is discretized by a finite element method, and deformations with a large displacement of the plate are handled by the corotational scheme (Doyle 2001). More details on numerical methods can be found in our previous papers (Hua *et al.* 2013; Huang, Wei & Lu 2018; Zhang, Huang & Lu 2020).

To validate the numerical method, a single plate in isolated swimming (Zhu *et al.* 2014a) was simulated with $Re = 200$, $h_0^* = 0.5$, $M^* = 0.2$, $K^* = 0.8$ and $S^* = 1000$. In the simulations, the computational domain for fluid flow is chosen as $[-15, 25] \times [-15, 15]$
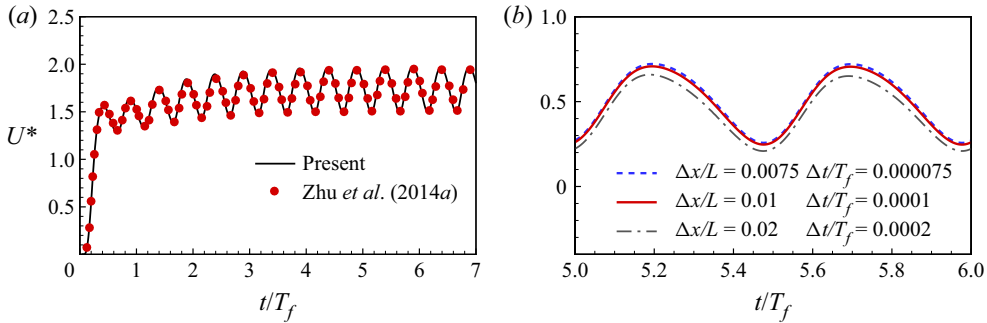
Figure 2. (*a*) Validation for the case of a self-propelled heaving plate with the non-dimensional governing parameters: $Re = 200$, $h_0^* = 0.5$, $M^* = 0.2$, $K^* = 0.8$ and $S^* = 1000$ (Zhu, He & Zhang 2014*a*). (*b*) Grid independence and time-step independence studies for a self-propelled pitching plate with $K^* = 1$, $f^* = 1.0$, $\theta_0 = 20°$ and $Re_c = 100$. The streamwise velocity of the leading edge as a function of time is presented.

Case	Mesh and time step	U^*	P^*
$Re_c = 350$	$\Delta x_0 = 0.01$, $\Delta t_0/T_f = 0.0001$	1.75	1.32
	$\Delta x_1 = 0.0075$, $\Delta t_1/T_f = 0.000075$	1.77	1.33
	$\Delta x_2 = 0.0066$, $\Delta t_2/T_f = 0.000066$	1.78	1.33
$Re_c = 860$	$\Delta x_0 = 0.01$, $\Delta t_0/T_f = 0.0001$	4.35	12.48
	$\Delta x_1 = 0.0075$, $\Delta t_1/T_f = 0.000075$	4.45	12.53
	$\Delta x_2 = 0.0066$, $\Delta t_2/T_f = 0.000066$	4.48	12.55

Table 1. Grid independence and time-step independence studies for two typical cases with larger Re_c. Case1: $Re_c = 350$ ($K^* = 1$, $f^* = 1$, $h_0^* = 0.5$). Case2: $Re_c = 860$ ($K^* = 5$, $f^* = 2$, $h_0^* = 0.5$). The cruising speed U^* and input power P^* are presented.

in the x and y directions, which is sufficiently large so that the blocking effects of the boundaries are eliminated. A constant pressure with $\mathbf{v} = 0$ is imposed at all boundaries except for the outlet where $\partial \mathbf{v}/\partial x = 0$ with constant pressure is imposed (Zou & He 1997). Initially, the fluid velocity field is zero in the entire computational domain. In the x and y directions the mesh is uniform with spacing $\Delta x = \Delta y = 0.01L$, where L is the dimensional length of the plate. The time step is $\Delta t = T_f/10\,000$ for the simulations of fluid flow and plate deformation, where $T_f = 1/f$ is the flapping period. Besides, a finite moving computational domain (Hua *et al.* 2013) is used in the x-direction to allow the plate to move for a sufficiently long time. As the plate travels one lattice in the x-direction, the computational domain is shifted, i.e. one layer is added at the inlet and another layer is removed at the outlet (Hua *et al.* 2013).

Figure 2(*a*) shows the streamwise velocity of the leading edge as a function of time. It is seen that the present result is consistent with that of Zhu *et al.* (2014*a*). The results of grid independence and time-step independence for the case of $Re_c = 100$ are shown in figure 2(*b*). It is seen that $\Delta x/L = 0.01$ and $\Delta t/T_f = 0.0001$ are sufficient to achieve accurate results. The results of grid and time-step independence studies for higher Re_c are presented in table 1. It is seen that $\Delta x/L = 0.01$ and $\Delta t/T_f = 0.0001$ are accurate enough for $Re_c = 350$, while $\Delta x = 0.0075$ and $\Delta t/T_f = 0.000075$ are better for $Re_c = 860$. Hence, in most of the present simulations (i.e. cases with $Re_c < 400$), $\Delta x/L = 0.01$ and $\Delta t/T_f = 0.0001$ were adopted. For the cases with larger Re_c (> 400), a finer mesh $\Delta x/L = 0.0075$ and a smaller time step $\Delta t/T_f = 0.000075$ were adopted.

Besides, our numerical strategy used in this study has been validated and successfully applied to investigate many flow problems, such as the coupling performance of tandem flexible inverted flags in a uniform flow (Huang *et al.* 2018), the effect of the trailing-edge shape on the self-propulsive performance of heaving flexible plates (Zhang *et al.* 2020) and the intermittent locomotion performance of a self-propelled flapping plate (Liu, Huang & Lu 2020).

4. Results and discussion

In present simulations, three main parameters are fixed, namely, the Reynolds number $Re = 200$, mass ratio $M^* = 0.2$ and stretching stiffness $S^* = 1000$, which are identical to those in the previous studies (Zhu *et al.* 2014a; Peng *et al.* 2018a; Liu *et al.* 2020). Note that S^* is large enough so that the plate is almost inextensible. While other key parameters are variable, i.e. the bending stiffness $K^* \in [0.5, 10]$, the heaving amplitude $h_0^* \in [0.1, 0.5]$, the pitching amplitude $\theta_0 \in [5, 30]$ (deg.) and the flapping frequency $f^* \in [0.5, 2]$. It is noted that for real fish, $K^* \approx O(1)$, e.g. K^* of the tail fin of a goldfish (*Carassius auratus*) is within the range of 2.5–23 (Hua *et al.* 2013; Peng, Huang & Lu 2018b). Hence, $K^* \in [0.5, 10]$ is adopted here. In the following discussion, variables with a superscript '$*$' are dimensionless variables. The symbol '$\sim$' means that the two variables on the left and right-hand sides are proportional, and their dimensions are not necessarily consistent.

4.1. *Propulsive performances and scaling laws*

The mean propulsive speed U, thrust T and input power P are paid special attention. Specifically, U is calculated by the time-averaged speed of the leading edge ($s = 0$) within one cycle at the equilibrium state (Zhu *et al.* 2014a; Peng *et al.* 2018a), i.e.

$$U = \frac{1}{T_f} \int_{t'}^{t'+T_f} u(t)\,\mathrm{d}t = -\frac{1}{T_f} \int_{t'}^{t'+T_f} \left(\left. \frac{\partial X}{\partial t} \right|_{s=0} \right) \mathrm{d}t, \tag{4.1}$$

Here $u(t)$ is the instantaneous horizontal speed of the leading edge of the platea and P is defined as (Zhu *et al.* 2014a)

$$P = \frac{1}{T_f} \int_{t'}^{t'+T_f} P(t)\,\mathrm{d}t = \frac{1}{T_f} \int_{t'}^{t'+T_f} \left[\int_0^1 \mathbf{F}_r(s,t) \cdot \frac{\partial X(s,t)}{\partial t} \mathrm{d}s \right] \mathrm{d}t, \tag{4.2}$$

where $\mathbf{F}_r$ represents the force on the surrounding fluid by the plate.

The thrust and drag are defined based on force decomposition. The Lagrangian force $\mathbf{F}_s$, exerted on the plate by the surrounding fluid, can be decomposed into two parts: one is the normal force $\mathbf{F}^n$, in which the pressure component dominates; the other is the tangential force $\mathbf{F}^\tau$, which mainly comes from the viscous effects. These forces at the ith Lagrangian node are defined as follows (Peng *et al.* 2018a; Liu *et al.* 2020):

$$\mathbf{F}_{s,i} = [-p\mathbf{I} + \mathbf{T}] \cdot \mathbf{n} = \mathbf{F}_i^n + \mathbf{F}_i^\tau, \tag{4.3}$$

$$\mathbf{F}_i^n = \left(\mathbf{F}_{s,i} \cdot \mathbf{n} \right) \mathbf{n} = \left(F_{x,i}^n, F_{y,i}^n \right), \tag{4.4}$$

$$\mathbf{F}_i^\tau = \left(\mathbf{F}_{s,i} \cdot \boldsymbol{\tau} \right) \boldsymbol{\tau} = \left(F_{x,i}^\tau, F_{y,i}^\tau \right), \tag{4.5}$$

where $\mathbf{I}$ is the unit tensor, $\mathbf{T}$ is the viscous stress tensor, $\boldsymbol{\tau}$ is the unit tangential vector toward the trailing edge, $\mathbf{n}$ is the unit normal vector and $[\cdot]$ denotes the jump in
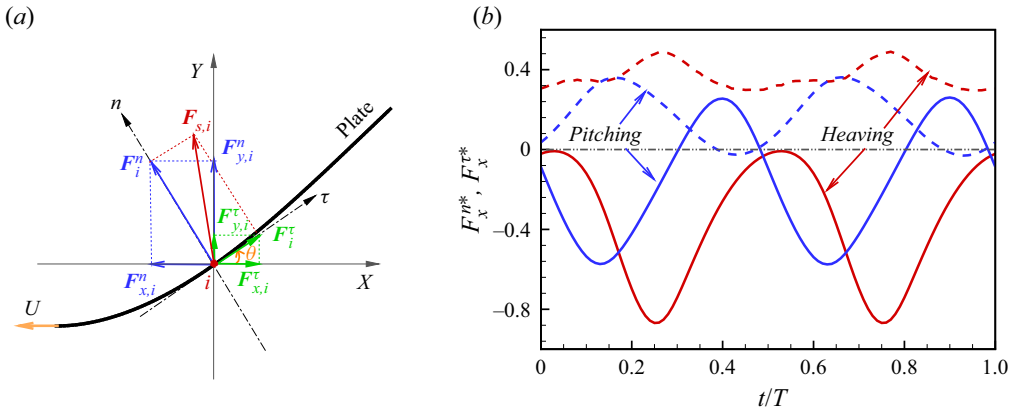
(*a*)

(*b*)

Figure 3. (*a*) Schematic diagram for force decomposition. Black curved line represents the plate. Red dot represents the *i*th Lagrangian node. Here τ and $\boldsymbol{n}$ denote the local tangential and normal vectors, respectively, and θ is the angle between τ and the positive direction of the *x*-axis. (*b*) The total dimensionless *x*-component of $\boldsymbol{F}^n$ and $\boldsymbol{F}^\tau$ (i.e. $F_x^n = \sum_i F_{x,i}^{n*}$ and $F_x^\tau = \sum_i F_{x,i}^{\tau*}$) for the pitching ($K^* = 1, \theta_0 = 20°, f^* = 1.0$) and heaving ($K^* = 1, h_0^* = 0.5, f^* = 1.0$) plates as functions of time within one flapping period. Solid and dashed lines represent F_x^{n*} and $F_x^{\tau*}$, respectively. The forces are normalized by $F_{ref} = \frac{1}{2}\rho U_{ref}^2 L$.

a quantity across the immersed boundary. Figure 3(*a*) shows the schematic diagram for force decomposition. The total *x*-component of $\boldsymbol{F}^n$ and $\boldsymbol{F}^\tau$ are $F_x^n = \sum_i F_{x,i}^n$ and $F_x^\tau = \sum_i F_{x,i}^\tau$, respectively. Figure 3(*b*) presents the dimensionless forces F_x^{n*} and $F_x^{\tau*}$ as functions of time within one cycle. It is seen that, for the heaving plate, F_x^n contributes much to a thrust since $F_x^n < 0$, while F_x^τ contributes to a drag for $F_x^\tau > 0$. However, for the pitching plates, F_x^n may contribute to a drag and F_x^τ may contribute to a thrust at some time. Hence, the thrust *T* and drag *D* can be defined as (Bottom *et al.* 2016)

$$-T(t) = \tfrac{1}{2}\left(F_x^n - |F_x^n|\right) + \tfrac{1}{2}\left(F_x^\tau - |F_x^\tau|\right), \left.\right\}$$
$$D(t) = \tfrac{1}{2}\left(F_x^n + |F_x^n|\right) + \tfrac{1}{2}\left(F_x^\tau + |F_x^\tau|\right). \quad (4.6)$$

The time-averaged thrust and drag are defined as $T = (1/T_f) \int_{t'}^{t'+T_f} T(t)\,\mathrm{d}t$ and $D = (1/T_f) \int_{t'}^{t'+T_f} D(t)\,\mathrm{d}t$, respectively.

The propulsive performances of the plates with the bending stiffness $K^* = 1$ are investigated first, as shown in figure 4. It is seen that U, T and P all increase with the increase of the flapping amplitude and frequency for both pitching and heaving plates. This is because that, generally, larger flapping amplitude and frequency mean that the plate may consume more energy, achieve larger thrust and be propelled faster. Besides, we have checked parameters of all cases in the present study and found that, for most of the cases, the flapping frequency f is significantly below the first natural frequency f_1 of the system. For the other few cases, even when the frequency ratio $f_r = f/f_1$ is larger than unity, it is close to unity. Hence, our result shows that when $f < f_1$, the speed, thrust and power increase monotonically with frequency. That is consistent with the results in the literature (Ramananarivo *et al.* 2011).

Actually, besides the effects of θ_0 (h_0^*) and f^*, the bending stiffness K^* may also have a significant effect on the performances of the plate (Peng *et al.* 2018*a*; Liu *et al.* 2020). Hence, it is necessary to adopt new parameters to concisely describe the results with different K^*, h_0^* or θ_0 and f^*. Inspired by previous works (Vandenberghe *et al.* 2004;
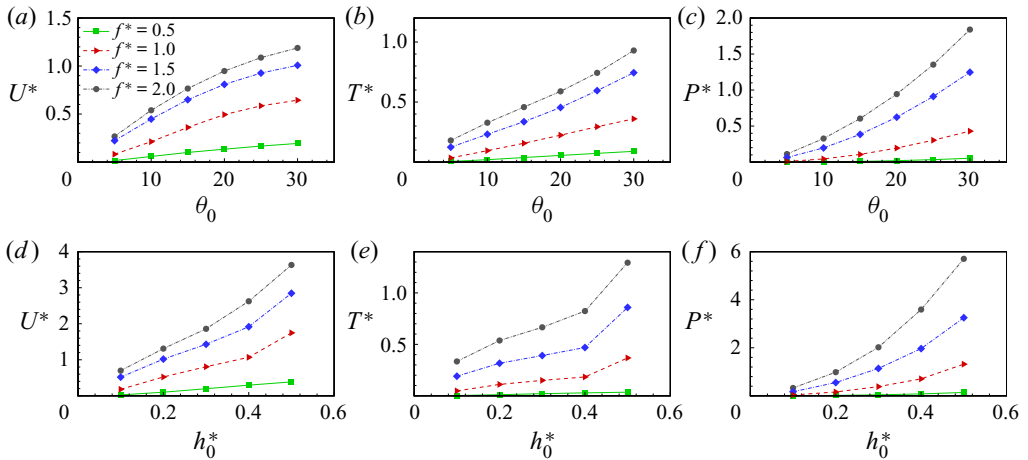
Figure 4. (*a*) Dimensionless propulsive speed U^*, (*b*) dimensionless thrust T^* and (*c*) dimensionless input power P^* as functions of flapping amplitude for pitching plates with different flapping frequency. Panels (*d*–*f*) are the corresponding results for heaving plates. In all these cases, $K^* = 1$. The velocity, force and power are normalized by $U_{ref} = \mu Re/(\rho L)$, $F_{ref} = (1/2)\rho U_{ref}^2 L$ and $P_{ref} = \rho U_{ref}^3 L$, respectively.

Gazzola *et al.* 2014; Lin *et al.* 2021), the flapping Reynolds number $Re_f = 2\pi f A_t L/\nu$ is introduced (i.e. the swimming number Sw in the study of Gazzola *et al.* 2014). Besides, the cruising Reynolds number $Re_c = UL/\nu$, based on the cruising speed U, can be defined.

The cruising Reynolds number Re_c as a function of Re_f is presented in figure 5. It is astonishing to see that, for both pitching and heaving plates, Re_c values of all cases follow the same scaling law approximately, i.e. $Re_c \sim Re_f^{3/2}$. This can be interpreted as follows. By a simple dimensional analysis reasoning (see Appendix A.1) and the elongated-body theory (EBT) (Lighthill 1960, 1971) (see Appendix A.2), we get that the thrust scaling is $T \sim (fA_t)^2$. This scaling is also identical to that in previous studies, e.g. Gazzola *et al.* (2014) and Quinn *et al.* (2014). As for the drag scaling, ample evidence (including theoretical analysis, experiments and simulations) indicates that, for a flexible body in an oncoming flow, D is proportional to $U^{4/3}$ (Alben *et al.* 2002; Zhu 2008; Luhar & Nepf 2011). In Appendix B, we further show that this drag scaling is still valid for the inclined plates, which are more like our flexible plates. More detailed discussions about the thrust and drag scaling are presented in § 4.2. Balancing the thrust and drag, one can get that $U^{4/3} \sim (fA_t)^2$, i.e. $U \sim (fA_t)^{3/2}$. From the definitions of Re_c and Re_f, the formula can be further written as $Re_c \sim Re_f^{3/2}$. The result is highly consistent with our observation from figure 5.

We would like to check whether the present scaling law is supported by the biological observations. Figure 6 shows that our scaling law is consistent with the biological data from the supplementary information of Gazzola *et al.* (2014). Meanwhile, the present scaling law seems to be applicable to a wider range of Re_f (up to $\sim 2.5 \times 10^5$).

Next, our scaling laws for the thrust T and the drag D are discussed. Figure 7 plots the dimensionless thrust T^* vs Re_f and the dimensionless drag D^* vs U^*. It is seen that there also exist some scaling laws. For the pitching plates, T^* (figure 7*a*) is proportional to $Re_f^{1.8}$ and D^* (figure 7*c*) is proportional to $U^{*1.2}$. While for heaving plates, T^* and D^* (see figure 7*b,d*) show approximately $Re_f^{2.1}$ and $U^{*1.4}$ growth, respectively. It is surprising to find that the thrust and drag scaling are very close to $T^* \sim Re_f^2$ and $D^* \sim U^{*4/3}$,
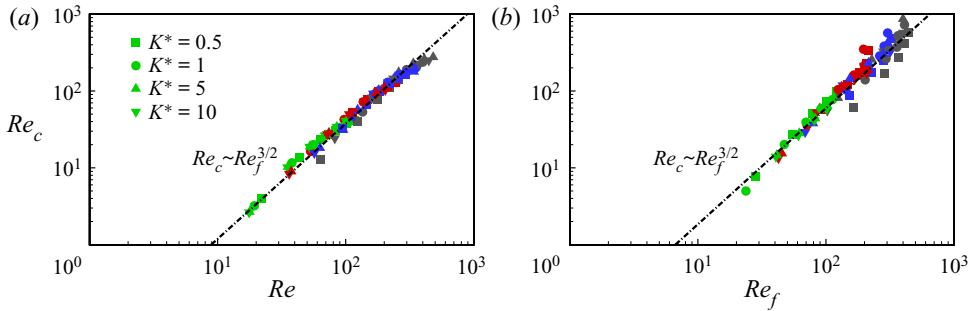
Figure 5. The cruising Reynolds number Re_c as a function of the flapping Reynolds number Re_f for (*a*) pitching and (*b*) heaving plates. Each symbol denotes a case that we simulated. Each kind of symbol represents the cases with a specific K. The green, red, blue and black symbols represent the cases with $f = 0.5$, 1.0, 1.5 and 2.0, respectively.
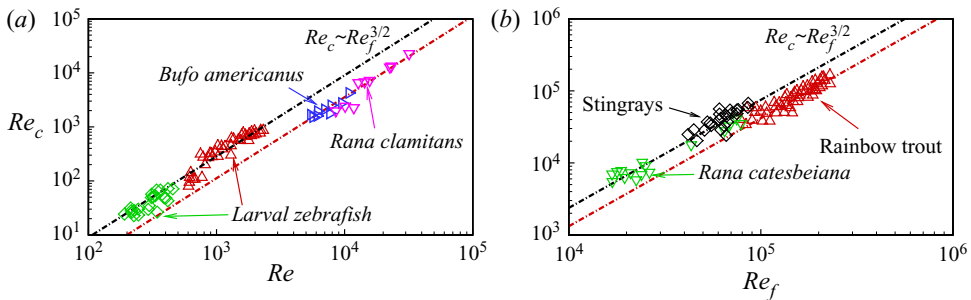

Figure 6. Biological data and the scaling $Re_c \sim Re_f^{3/2}$. The data sets are obtained from figures S4(*d*), S5(*d*), S8(*c*) and S10(*a,b*) in the supplementary information of Gazzola *et al.* (2014).

respectively, which we adopted above. Besides, due to $T = D$ at equilibrium state, one can get that $Re_f^{1.8} \sim U^{*1.2}$ for the pitching plates and $Re_f^{2.1} \sim U^{*1.4}$ for the heaving plates, which can both be further transformed to $Re_c \sim Re_f^{3/2}$. This confirms the scaling law in figure 5 from another view. It is also noticed that there is a small discrepancy between the numerical and theoretical scalings. This may be due to the nonlinearity of the system and the complex fluid–structure interaction, which are greatly simplified in the theoretical analyses. For example, in the theoretical analysis (see Appendix A), we assumed that the effect of stiffness K^* is fully included in A_t.

It is seen that the data sets of T and D for the pitching plates overlap very well (figure 7*a,c*). Note that due to the flexibility of the plate, the direct result is the emergence of the passive pitching angle θ_p (see figure 1). Nevertheless, the locomotion style has not changed for the pitching plates (compared with the heaving plates, see below). Under the same locomotion style, the growing forms of T and D should be identical. Therefore, all pitching data sets collapse into a single curve.

On the other hand, for the flexible heaving plates, there are both heaving (active, amplitude h_0) and pitching (passive, amplitude θ_p) motions. When the plate is almost rigid, the heaving motion is prominent. When the plate becomes more flexible, the passive pitching motion becomes more prominent, i.e. there may be a large θ_p. Actually, here
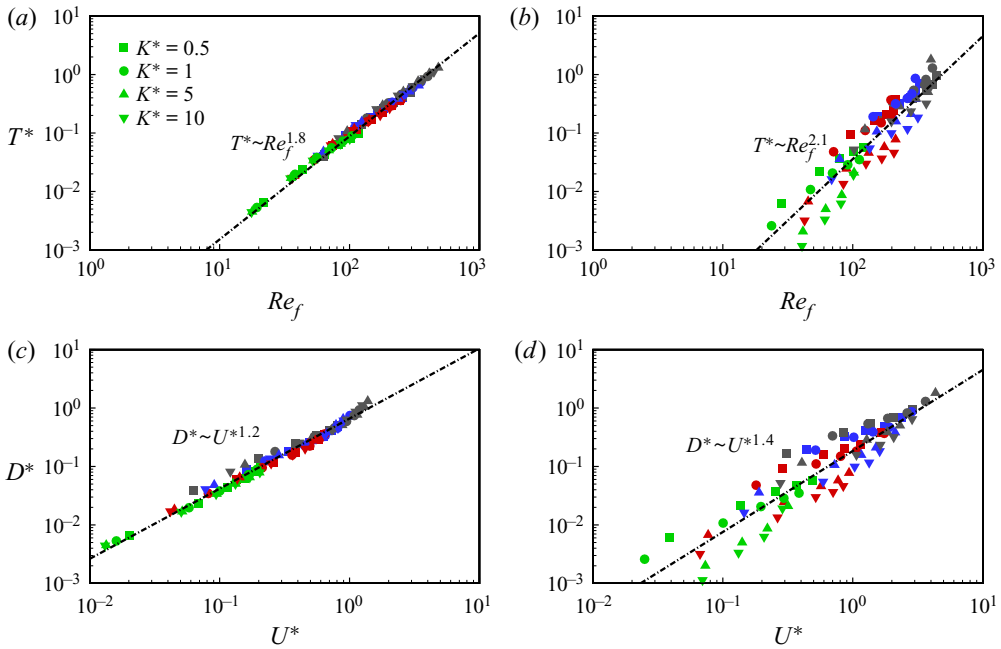
Figure 7. (*a*) The dimensionless thrust T^* as a function of Re_f and (*c*) the dimensionless drag D^* as a function of U^* for pitching plates. Panels (*b,d*) are the corresponding results of the heaving plates. Symbols are identical to those in figure 5. The velocity and force are normalized by $U_{ref} = \mu Re/\rho L$ and $F_{ref} = (1/2)\rho U_{ref}^2 L$, respectively.

K^* plays an important role in the thrust generation. For the rigid plate, the thrust is mainly generated by the leading-edge vortex (Vandenberghe *et al.* 2004), while for the flexible plate, the normal force contributes much to the thrust (Peng *et al.* 2018*a*; Liu *et al.* 2020). Due to the different flow mechanism, the flexibility influences the thrust scaling considerably (and drag scaling, since $T = D$). Therefore, the data sets do not overlap very well. It is also noticed that T at smaller K^* (i.e. $K^* = 0.5$ and 1, the square and circle symbols in figure 7*b*) is higher than that at larger K^* (i.e. $K^* = 5$ and 10). This is because the thrust can be significantly enhanced by appropriately increasing the flexibility (Marais *et al.* 2012).

Finally, the power expended is considered, as presented in figure 8. Results show that the dimensionless input power P^* can be scaled as $P^* \sim Re_f^{2.7}$ for both pitching and heaving plates, which is consistent with the results of Quinn *et al.* (2014). Besides, as described in the introduction, Floryan *et al.* (2018) showed that the power scaling is $P \sim fL(V^2 - V_h V_\theta)$. Note that $V_h V_\theta = 0$ in the present study, hence $P \sim fLV^2 \sim fL(fA_t)^2$. If the flapping amplitude is large, i.e. $A_t \sim L$, the formula becomes $P \sim (fA_t)^3$. The same power scaling can also be obtained by dimensional analysis (see Appendix A.1). In the derivation, if A_t is large, the effect of lateral velocity fA_t is more significant and therefore more suitable to be chosen as the characteristic velocity. The derivation from the EBT of Lighthill (1971) also confirms our power scaling (see Appendix A.2). On the other hand, for small amplitude, i.e. $A_t/L \ll 1$, the model of Theodorsen (1935) indicates $P \sim (fA_t)^2$. It is noticed that in our study, $A_t/L \in [0.09, 0.55]$. Therefore, the amplitude in our study is moderate, which is between the conditions $A_t/L \ll 1$ and $A_t \sim L$.
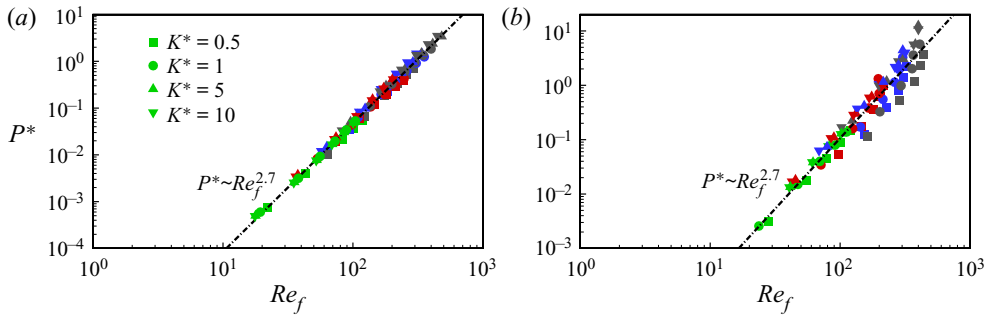
936 A9-10

Figure 8. The dimensionless time-average input power P^* as a function of Re_f for the (*a*) pitching plates and (*b*) heaving plates. Symbols as in figure 5. The powers are normalized by $P_{ref} = \rho U_{ref}^3 L$.

Therefore, approximately the exponent should between two and three. In the experimental study of rigid tethered pitching foils by Quinn *et al.* (2014), their flapping amplitude range is $A_t/L \in [0.095, 0.16]$ and they have $P \sim (fA_t)^{2.7}$. In general, our A_t range is a little bit larger than that of Quinn *et al.* (2014). The exponent should be closer to three. However, compared with the rigid foils, our flexible plates should be favourable for energy consumption (Zhu *et al.* 2014*b*). Hence, the power scaling of a flexible foil with larger A_t may be close to that of the rigid foil with smaller A_t. In other words, our power scaling $(fA_t)^{2.7}$ is reasonable.

4.2. *Comparison with results in the literature*

In the above, we proposed a new scaling law, i.e. $Re_c \sim Re_f^{3/2}$. It is also noted that other two scaling laws, namely, $Re_c \sim Re_f^{4/3}$ and $Re_c \sim Re_f^{5/3}$, are given by Gazzola *et al.* (2014) and Lin *et al.* (2021), respectively. In the following, we would like to make a thorough comparison between these scaling laws.

Indeed, the three scaling laws may look close in the qualitative analysis of a log–log plot. However, a quantitative analysis of our data fittings indicates that the optimal Re_c-scaling is $Re_c \sim Re_f^{3/2}$ with $R^2 = 0.99$ for the pitching cases (figure 5*a*) and $R^2 = 0.97$ for the heaving cases (figure 5*b*).

Besides, note that all three scaling laws can be derived from the balance of thrust and drag. Hence, a more essential analysis should start from thrust and drag scaling. Gazzola *et al.* (2014) have derived a scaling law of thrust T, i.e. $T \sim (fA_t)^2$. The thrust scaling has been found and confirmed further in other studies (Quinn *et al.* 2014; Floryan *et al.* 2018; Gibouin *et al.* 2018; Van Buren *et al.* 2018) and our physical reasoning (see Appendix A). In addition, the quantitative results of T in figures 7(*a*) and 7(*b*) are also consistent well with this thrust scaling.

Under the circumstances of $T \sim (fA_t)^2$, the swimming speed scale is sensitive to the assumed drag law. For the drag scaling, Gazzola *et al.* (2014) suggested that $D \sim U^{3/2}$, which is estimated from the viscous drag on a flat and rigid plate aligned with the flow. However, for a real fish, due to its flexibility, when it flaps, its body continuously deforms. The curved boundary layer and the corresponding drag should be quite different from those of the rigid flat plate. Therefore, the drag scaling of Gazzola *et al.* (2014) may be not universally applicable. The flexible curved boundary-layer effect has been fully considered in previous studies and found that a stationary curved flexible fibre or plate in an oncoming flow experiences a drag proportional to $U^{4/3}$ (Alben *et al.* 2002; Zhu 2008;

Gosselin *et al.* 2010; Luhar & Nepf 2011). Generally speaking, $U^{4/3}$ scaling denotes a drag reduction for flexible curved plates (Alben *et al.* 2002). Besides, as we have shown in Appendix B, the $U^{4/3}$ scaling is still valid for inclined plates, whose shapes are also curved and streamlined due to deformation. Therefore, in the present study, the drag of the deformed curved flapping plates should be close to that of plates in Alben *et al.* (2002), rather than that of flat plates. Moreover, it can be observed directly from figures 7(*c*) and 7(*d*) that the $U^{4/3}$ scaling of drag can fit our data well. Hence, it is adopted to perform the analysis.

In summary, there are strong grounds to support our scalings $T \sim (fA_t)^2$ and $D \sim U^{4/3}$, and further support the scaling $Re_c \sim Re_f^{3/2}$.

In the study of Lin *et al.* (2021), the drag scaling of Gazzola *et al.* (2014), i.e. $D \sim U^{3/2}$, was adopted. They then derived a new thrust scaling, i.e. $T \sim (fA_t)^{5/2}$. However, the new thrust scaling has never been confirmed or validated yet. One might conjecture that the thrust scaling is only applicable to their rigid self-propulsive flapping model.

It should be pointed out that Re in the present study is close to that of larvae. Although our Re is much lower than those of many adult swimming animals, our scaling may extend to surprisingly higher Re (up to $\sim 2.5 \times 10^5$, see figure 6). While Re in the study of Gazzola *et al.* (2014) went up past 10^8, around 1000 higher than what is presented here. Indeed, Re may impact the nature of drag. If Re is high enough, biological data may switch to a different scaling.

5. Conclusions

The propulsive performances of self-propelled flapping flexible plates are investigated numerically. Both pitching and heaving motions are considered. Results indicate that the propulsive speed U, thrust T and input power P increase with the flapping amplitude and frequency in both locomotion styles. Further, some simple scaling laws are found. Specifically, for both pitching and heaving plates, the cruising Reynolds number Re_c can be scaled as $Re_c \sim Re_f^{3/2}$, and the dimensionless input power P^* can be scaled as $P^* \sim Re_f^{2.7}$. The scaling laws of T and P are also derived using dimensional analysis reasoning and the EBT (Lighthill 1971). The derived laws are consistent with or close to our findings. For the thrust and drag calculated in our simulations, the scaling laws are very close to $(fA_t)^2$ and $U^{4/3}$, respectively. They are consistent with those in the literature. The $U^{4/3}$ drag law is found to be still applicable for inclined plates. Besides, the flexibility influences the thrust scaling considerably for the heaving plates, while it does not for the pitching plates. The Re_c scaling can be simply derived by balancing the thrust and drag. Our present scaling law is also well supported by biological data. This study may deepen our understanding of the locomotion of aquatic animals and may be helpful for bionic design.

Declaration of interests. The authors report no conflict of interest.

Author ORCIDs.

Kui Liu https://orcid.org/0000-0001-9897-6375;

Haibo Huang https://orcid.org/0000-0002-1308-9900.

Appendix A. Physical reasoning for the scaling laws

A.1. *Dimensional analysis reasoning for the thrust and power scalings*

Dimensional analysis reasoning is a broadly applicable technique for developing scaling laws. In isothermal fluid mechanics problems, there are only three basic dimensions, i.e. mass $\mathcal{M}$, length $\mathcal{L}$ and time $\mathcal{T}$. Therefore, only three repeating parameters are required, and the determinant of the dimensional matrix formed from these three parameters must be non-zero (Kundu, Cohen & Dowling 2012). The common choices are characteristic length, velocity and density. In the present flow system, the length of the plate L and the fluid density ρ are naturally chosen as characteristic length and density, respectively. For the characteristic velocity, there are two choices, i.e. the cruising speed U and fA_t based on the trailing-edge amplitude A_t. However, U is determined by the characteristic lateral velocity of the tail motion fA_t, i.e. the most important velocity scale is fA_t instead of U (Van Buren *et al.* 2018; Smits 2019). Hence, the characteristic velocity fA_t is adopted here.

It is noted that there are four variable dimensionless input parameters in our study, i.e. the bending stiffness K^*, the heaving amplitude h_0^*, the pitching amplitude θ_0 and the flapping frequency f^* (see § 4). Actually, the effects of these four parameters are directly or indirectly included in the characteristic velocity fA_t. Specifically, the flapping frequency f appears explicitly in fA_t; the amplitude of the trailing edge A_t is mainly affected by the flapping amplitude (h_0^* or θ_0) and modulated by the bending stiffness K^*. From this point of view, fA_t is indeed a key characteristic quantity of the system.

Hence, we assume that the effects of the flapping amplitude (h_0^* or θ_0) and the rigidity (K^*) can be all quantified by A_t as a whole. Through this assumption, we can get a much simpler form of scalings using only three parameters (i.e. ρ, L and fA_t). Besides, we finally get the same thrust scaling as that of Gazzola *et al.* (2014). Also note that in the experimental study about flexible flapping plates of Floryan, Van Buren & Smits (2019), when f is small (i.e. the Strouhal number $St = 2fA_t/U_\infty$ is small), the data of thrust and power are well collapsed (see their figures 8(*b*), 9(*b*), 10(*b*) and 11(*b*)). In other words, A_t can capture the effects of flexibility and describe the results well when f is small. Therefore, this assumption is reasonable to a certain extent. Indeed, A_t cannot fully represent the effect of K^*. As we have mentioned in § 4.1, this simplified analysis may lead to a small discrepancy between the numerical and theoretical scalings.

According to the Π theorem of Buckingham (1914), a dimensionless group of thrust is expressed as

$$\Pi_1 = T\rho^a(fA_t)^bL^c. \tag{A1}$$

Note that, for a two-dimensional problem, the dimensions of T, ρ, fA_t and L are $[T] = $ [N m^{-1}], $[\rho] = $ [kg m^{-3}], $[fA_t] = $ [m s^{-1}] and $[L] = $ [m], respectively. Since Π_1 is dimensionless, one can easily obtain that the exponents $a = -1$, $b = -2$ and $c = -1$. Therefore,

$$\Pi_1 = \frac{T}{\rho(fA_t)^2L}. \tag{A2}$$

Holding Π_1 constant, one can get that $T \sim (fA_t)^2$, i.e. $T^* \sim Re_f^2$ when written in dimensionless form.

As for the input power P, the dimensionless group is

$$\Pi_2 = P\rho^a(fA_t)^bL^c. \tag{A3}$$

The dimension of P is $[P] = [\text{kg m s}^{-3}]$ for a two-dimensional problem. Because Π_2 is dimensionless, it is easy to find that $a = -1$, $b = -3$ and $c = -1$. Hence,

$$\Pi_2 = \frac{P}{\rho(fA_t)^3 L}. \tag{A4}$$

Holding Π_2 constant, we have $P \sim (fA_t)^3$, which can be written in non-dimensional form as $P^* \sim Re_f^3$.

A.2. *Elongated-body theory for the scaling laws*

Elongated-body theory has been widely adopted in previous studies about two- and three-dimensional problems (Bottom *et al.* 2016; Floryan *et al.* 2018; Akbarzadeh & Borazjani 2019). For an undulating plate, the lateral motion of the whole body is expressed by the travelling-wave equation

$$Y(z, t) = A(z) \sin(2\pi ft - 2\pi z/\lambda), \tag{A5}$$

where $A(z)$ is the amplitude of the wave, z is the axial direction from the leading edge ($z = 0$) to the trailing edge ($z = L$), f is the frequency and λ is the wavelength. According to the EBT (Lighthill 1960, 1971), the thrust of an undulating plate is expressed as

$$T = \left[mw\left(W - \frac{1}{2}w\right)\right]_{z=L} - \frac{\partial}{\partial t}\int_0^L \left(mw\frac{\partial Y}{\partial z}\right) dz, \tag{A6}$$

where m is the virtual mass per unit length (Lighthill 1971; Akbarzadeh & Borazjani 2019). Note that for a three-dimensional body, $m = \frac{1}{4}\pi\beta\rho s^2$, where $\beta \approx 1$ is a non-dimensional parameter, ρ is the fluid density and s is the span (Lighthill 1971). For two-dimensional problems, although m may have a different expression, it is independent of kinematic parameters (i.e. f and A_t), i.e. we can take m as a constant. Hence, m does not affect the scaling laws. Here $W = \partial Y/\partial t = 2\pi fA(z) \cos(2\pi ft - 2\pi z/\lambda)$ is the lateral velocity of the plate, and $w = DY/Dt = \partial Y/\partial t + U(\partial Y/\partial z)$ is the lateral velocity of fluid adjacent to the plate. Using (A5) and assuming the variation of $A(z)$ along the axial direction is very small (especially near the trailing edge ($z = L$)), i.e. $A'(z) \approx 0$, we can get that

$$w = 2\pi fA(z)\left(1 - \frac{U}{f\lambda}\right)\cos(2\pi ft - 2\pi z/\lambda) = W\left(1 - \frac{U}{f\lambda}\right). \tag{A7}$$

Actually, just as indicated by Lighthill (1971), we have $w = W(V - U)/V$, where $V = f\lambda$ is the wave speed.

Note that the time-averaged value within one cycle of the integral item in (A6) is zero and $A(z) = A_t$ at $z = L$. Hence, (A6) becomes

$$T \sim m(fA_t)^2\left(1 - \left(\frac{U}{f\lambda}\right)^2\right). \tag{A8}$$

For the flapping plate in our study, there is no obvious undulation during swimming (see figure 1). In other words, λ is large in our flapping cases and the item $(U/f\lambda)$ may be small enough to be neglected. Hence, (A8) is reduced to $T \sim (fA_t)^2$.
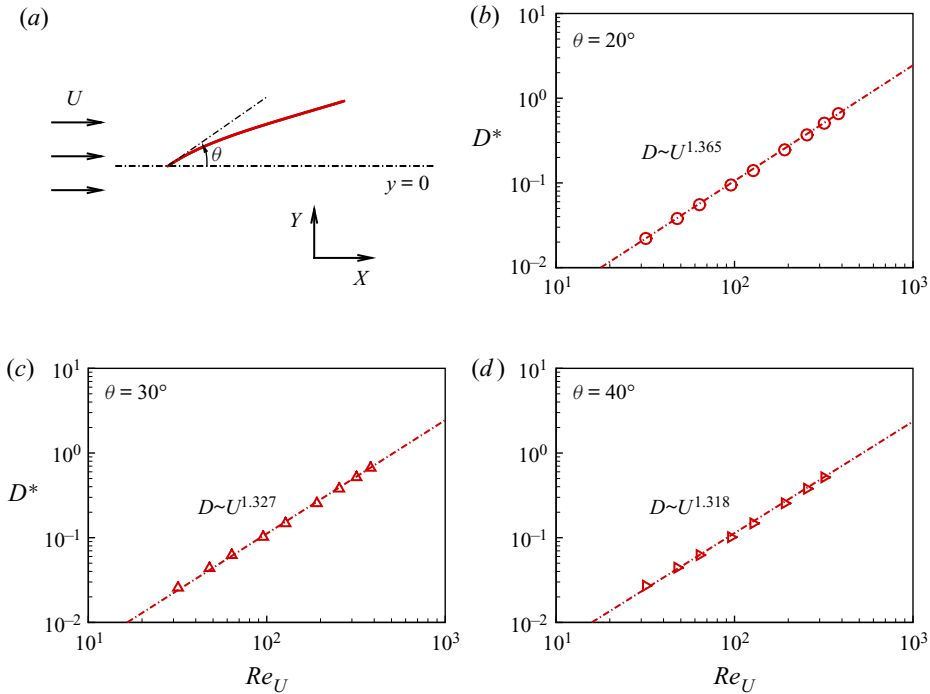
Figure 9. (*a*) Schematic diagram of the inclined plate in oncoming flow, where θ is the inclination angle of the plate and U is the oncoming flow velocity. (*b–d*) The dimensionless drag D^* of inclined plates as functions of Reynolds number ($Re_U = UL/\nu \sim U$) with different θ and bending stiffness K^*: (*b*) $\theta = 20°$, $K^* = 0.01$, (*c*) $\theta = 30°$, $K^* = 0.01$ and (*d*) $\theta = 40°$, $K^* = 0.005$.

We further estimate the power consumed by the plate. The acceleration of fluid adjacent to the plate is $a = \mathrm{D}w/\mathrm{D}t$. Considering $A'(z) \approx 0$, we have

$$a = -4\pi^2 f^2 A(z) \left(1 - \frac{U}{f\lambda}\right)^2 \sin(2\pi ft - 2\pi z/\lambda). \tag{A9}$$

Similarly, $A(L) = A_t$. Neglecting the item $(U/f\lambda)$, we have $a \sim f^2 A_t$. The mass of fluid pushed by the plate is scaled as ρLA_t. The plate does work at a rate equal to its lateral velocity $W \sim fA_t$. Hence, the power expenditure is scaled as $P \sim (\rho LA_t) \cdot (f^2 A_t) \cdot (fA_t)$, i.e. $P \sim (fA_t)^3$.

Appendix B. Drag scaling for the inclined plates

One may notice that the fibre in the study of Alben *et al.* (2002) is normal to the incoming flow, i.e. the inclination angle θ in figure 9(*a*) is 90°. For a fixed θ, i.e. in Alben's model, increased speed is associated with reduced projected frontal area. People may have an illusion that in the self-propulsive cases, the increased speed is associated with increased frontal area, which is opposite to Alben's cases. However, note that in our study, θ (i.e. pitching amplitude) is variable. Hence, it is unreasonable to directly compare the relationship between speed and projected frontal area. Nevertheless, we would like to illustrate why Alben's drag law can be applied in our study.

First, we try to test whether the drag scaling of Alben *et al.* (2002) can be applied to the cases with different fixed inclination angle θ (see figure 9(*a*)), since our flexible
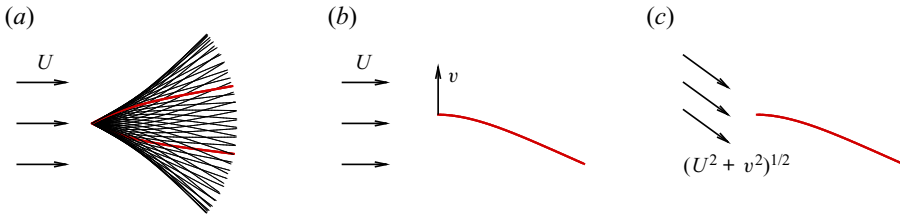
(*a*) (*b*) (*c*)

Figure 10. The pitching (*a*) and heaving (*b*) plates in an inertial frame. (*c*) The heaving plate in a non-inertial frame moving with the head of the plate.

plates are more like inclined plates (see figure 1). Here many cases for different θ and bending rigidity K^* are simulated. The computational domain, grid spacing and time step are identical to these in § 3. The oncoming flow velocity is U and the Reynolds number is $Re_U = UL/\nu$. The horizontal force experienced by the plate is the drag D. Note that, under these circumstances, the plate is completely passive and K^* should be relatively small to ensure that the bending deformation of the plate is relatively large (Alben *et al.* 2002; Zhu 2008), so that the plate shape is more streamlined.

The dimensionless drag D^* as a function of Re_U for cases of different θ and K^* are presented in figure 9(*b–d*). It is seen that the growing forms of drag are very close to that of Alben *et al.* (2002) (i.e. $D \sim U^{4/3}$). In other words, even when the plate is inclined, Alben's law is still valid. Therefore, if a flexible plate has a streamlined curved shape in an oncoming flow due to the fluid–structure interaction (FSI), $U^{4/3}$ drag law seems applicable. This may be regarded as a simple generalization of Alben's drag law.

Besides, we can change our views on the pitching and heaving cases in new inertial and non-inertial frames, respectively, to see the analogies between our cases and those of Alben *et al.* (2002).

For a pitching plate, because the cruising speed U is almost a constant, we can view the locomotion in an inertial frame (see figure 10*a*) which is moving with U. In the new frame, at any time, the oncoming flow with U is passing through an inclined flexible plate. It is noticed in the inertial frame, except the head of the plate experiences a rotational moment, the other part of the plate is free to move passively and form a streamlined shape due to the FSI. According to this viewpoint, Alben's law can be applied.

For a heaving plate, suppose the cruising speed is U. In the inertial frame which is moving with U, the plate is heaving up and down (see figure 10*b*). We can set up a non-inertial frame moving with the head of the plate. Suppose at time t, the plate moves upward with a lateral component velocity v. In this new frame, we can see that the inclined oncoming flow with velocity magnitude $\sqrt{U^2 + v^2}$ is passing through the flexible plate (see figure 10*c*). It is easy to imagine that at different times during a period, the oncoming flow from different angles is passing through the flexible plate. In the non-inertial frame, except the head of the plate experiences an inertia force, the other part of the plate is free to move passively and form a streamlined shape due to the FSI. According to this viewpoint, Alben's law should also be valid in this situation.

REFERENCES

AKBARZADEH, A.M. & BORAZJANI, I. 2019 Reducing flow separation of an inclined plate via travelling waves. *J. Fluid Mech.* **880**, 831–863.

ALBEN, S., SHELLEY, M. & ZHANG, J. 2002 Drag reduction through self-similar bending of a flexible body. *Nature* **420**, 479–481.

ALBEN, S., SHELLEY, M. & ZHANG, J. 2004 How flexibility induces streamlining in a two-dimensional flow. *Phys. Fluids* **16**, 1694–1713.

BATCHELOR, G.K. 1967 *An Introduction to Fluid Dynamics*. Cambridge University Press.

BOTTOM, R.G. II, BORAZJANI, I., BLEVINS, E.L. & LAUDER, G.V. 2016 Hydrodynamics of swimming in stingrays: numerical simulations and the role of the leading-edge vortex. *J. Fluid Mech.* **788**, 407–443.

BUCKINGHAM, E. 1914 On physically similar systems; illustrations of the use of dimensional equations. *Phys. Rev.* **4**, 345–376.

CONNELL, B.S.H. & YUE, D.K.P. 2007 Flapping dynamics of a flag in a uniform stream. *J. Fluid Mech.* **581**, 33–67.

DAI, L., HE, G., ZHANG, X. & ZHANG, X. 2018 Intermittent locomotion of a fish-like swimmer driven by passive elastic mechanism. *Bioinspir. Biomim.* **13**, 056011.

DEWEY, P.A., BOSCHITSCH, B.M., MOORED, K.W., STONE, H.A. & SMITS, A.J. 2013 Scaling laws for the thrust production of flexible pitching panels. *J. Fluid Mech.* **732**, 29–46.

DOYLE, J.F. 2001 *Nonlinear Analysis of Thin-Walled Structures: Statics, Dynamics, and Stability*. Springer.

FLORYAN, D. & ROWLEY, C.W. 2018 Clarifying the relationship between efficiency and resonance for flexible inertial swimmers. *J. Fluid Mech.* **853**, 271–300.

FLORYAN, D., VAN BUREN, T., ROWLEY, C.W. & SMITS, A.J. 2017 Scaling the propulsive performance of heaving and pitching foils. *J. Fluid Mech.* **822**, 386–397.

FLORYAN, D., VAN BUREN, T & SMITS, A.J. 2018 Efficient cruising for swimming and flying animals is dictated by fluid drag. *Proc. Natl Acad. Sci. USA* **115**, 8116–8118.

FLORYAN, D., VAN BUREN, T & SMITS, A.J. 2019 Performance and scaling of flexible inertial swimmers. In *11th International Symposium on Turbulence and Shear Flow Phenomena*.

GAZZOLA, M., ARGENTINA, M. & MAHADEVAN, L. 2014 Scaling macroscopic aquatic locomotion. *Nat. Phys.* **10**, 758–761.

GIBOUIN, F., RAUFASTE, C., BOURET, Y. & ARGENTINA, M. 2018 Study of the thrust–drag balance with a swimming robotic fish. *Phys. Fluids* **30** (9), 091901.

GOSSELIN, F., DE LANGRE, E. & MACHADO-ALMEIDA, B.A. 2010 Drag reduction of flexible plates by reconfiguration. *J. Fluid Mech.* **650**, 319–341.

HUA, R.-N., ZHU, L. & LU, X.-Y. 2013 Locomotion of a flapping flexible plate. *Phys. Fluids* **25**, 121901.

HUANG, H., WEI, H. & LU, X.-Y. 2018 Coupling performance of tandem flexible inverted flags in a uniform flow. *J. Fluid Mech.* **837**, 461–476.

KANG, C.-K., AONO, H., CESNIK, C.E.S. & SHYY, W. 2011 Effects of flexibility on the aerodynamic performance of flapping wings. *J. Fluid Mech.* **689**, 32–74.

KUNDU, P.K., COHEN, I.M. & DOWLING, D.R. 2012 *Fluid Mechanics*. Academic Press.

LAUDER, G.V. 2015 Fish locomotion: recent advances and new directions. *Annu. Rev. Mar. Sci.* **7**, 521–545.

LIGHTHILL, M.J. 1960 Note on the swimming of slender fish. *J. Fluid Mech.* **9** (2), 305–317.

LIGHTHILL, M.J. 1971 Large-amplitude elongated-body theory of fish locomotion. *Proc. R. Soc. Lond.* **179**, 125–138.

LIN, X., WU, J. & ZHANG, T. 2021 Self-directed propulsion of an unconstrained flapping swimmer at low Reynolds number: hydrodynamic behaviour and scaling laws. *J. Fluid Mech.* **907**, R3.

LIU, K., HUANG, H. & LU, X.-Y. 2020 Hydrodynamic benefits of intermittent locomotion of a self-propelled flapping plate. *Phys. Rev.* E **102**, 053106.

LUHAR, M. & NEPF, H.M. 2011 Flow-induced reconfiguration of buoyant and flexible aquatic vegetation. *Limnol. Oceanogr.* **56** (6), 2003–2017.

MARAIS, C., THIRIA, B., WESFREID, J.E. & GODOY-DIANA, R. 2012 Stabilizing effect of flexibility in the wake of a flapping foil. *J. Fluid Mech.* **710**, 659–669.

MITTAL, R. & IACCARINO, G. 2005 Immersed boundary methods. *Annu. Rev. Fluid Mech.* **37** (1), 239–261.

PENG, Z.-R., HUANG, H. & LU, X.-Y. 2018a Collective locomotion of two closely spaced self-propelled flapping plates. *J. Fluid Mech.* **849**, 1068–1095.

PENG, Z.-R., HUANG, H. & LU, X.-Y. 2018b Hydrodynamic schooling of multiple self-propelled flapping plates. *J. Fluid Mech.* **853**, 587–600.

PESKIN, C.S. 2002 The immersed boundary method. *Acta Numerica* **11**, 479–517.

QUINN, D.B., MOORED, K.W., DEWEY, P.A. & SMITS, A.J. 2014 Unsteady propulsion near a solid boundary. *J. Fluid Mech.* **742**, 152–170.

RAMANANARIVO, S., GODOY-DIANA, R. & THIRIA, B. 2011 Rather than resonance, flapping wing flyers may play on aerodynamics to improve performance. *Proc. Natl Acad. Sci. USA* **108**, 5964–5969.

SHOELE, K. & ZHU, Q. 2012 Leading edge strengthening and the propulsion performance of flexible ray fins. *J. Fluid Mech.* **693**, 402–432.

SMITS, A.J. 2019 Undulatory and oscillatory swimming. *J. Fluid Mech.* **874**, P1.

Theodorsen, T. 1935 *General Theory of Aerodynamic Instability and the Mechanism of Flutter*. National Advisory Committee for Aeronautics.

Thiria, B. & Godoy-Diana, R. 2010 How wing compliance drives the efficiency of self-propelled flapping flyers. *Phys. Rev.* E **82**, 015303.

Triantafyllou, M.S., Triantafyllou, G.S. & Yue, D.K.P. 2000 Hydrodynamics of fishlike swimming. *Annu. Rev. Fluid Mech.* **32**, 33–53.

Van Buren, T., Floryan, D., Wei, N. & Smits, A.J. 2018 Flow speed has little impact on propulsive characteristics of oscillating foils. *Phys. Rev. Fluids* **3**, 013103.

Vandenberghe, N., Zhang, J. & Childress, S. 2004 Symmetry breaking leads to forward flapping flight. *J. Fluid Mech.* **506**, 147–155.

Wootton, R.J. 1992 Functional morphology of insect wings. *Annu. Rev. Entomol.* **37**, 113–140.

Zhang, C., Huang, H. & Lu, X.-Y. 2020 Effect of trailing-edge shape on the self-propulsive performance of heaving flexible plates. *J. Fluid Mech.* **887**, A7.

Zhu, L. 2008 Scaling laws for drag of a compliant body in an incompressible viscous flow. *J. Fluid Mech.* **607**, 387–400.

Zhu, L. & Peskin, C.S. 2002 Simulation of a flapping flexible filament in a flowing soap film by the immersed boundary method. *J. Comput. Phys.* **179** (2), 452–468.

Zhu, X., He, G. & Zhang, X. 2014a Flow-mediated interactions between two self-propelled flapping filaments in tandem configuration. *Phys. Rev. Lett.* **113**, 238105.

Zhu, X., He, G. & Zhang, X. 2014b How flexibility affects the wake symmetry properties of a self-propelled plunging foil. *J. Fluid Mech.* **751**, 164–183.

Zou, Q. & He, X. 1997 On pressure and velocity boundary conditions for the lattice Boltzmann BGK model. *Phys. Fluids* **9** (6), 1591–1598.